


REVERSE ENGINEERING-INSPIRED PARAMETRIC 3D GEOMETRY MODEL OF MARINE PROPELLER

Long Zheng 

Shunhuai Chen* 

Xinyu Chen 

Shengchen Ji

School of Naval Architecture, Ocean and Energy Power Engineering, Wuhan University of Technology, Wuhan, China

Corresponding author: shchen@whut.edu.cn (Shunhuai Chen)

ABSTRACT

In this study, an effective parametric 3D geometry model of a propeller was established with the aid of reverse engineering. The goal is to reduce the free parameters while automating the modelling of the propeller. The process of building the parametric model begins by generating an initial point cloud by defining the feature matrix associated with the propeller blade profile shape. Subsequently, the initial point cloud is deformed and refined by the deformation feature matrix and resampling. Finally, a 3D geometry model of the propeller is generated by surface reconstruction. The model can be built automatically by interactively modifying the feature matrices. Two numerical analyses illustrate the performance of the parametric 3D geometry model. Specifically, two propellers are constructed using the proposed model to estimate the shape error between the reconstructed propellers and the original offset of the propellers. These propellers are selected as research objects to determine the hydrodynamic performance error between the propeller constructed by the proposed model and a benchmark propeller. According to the results of the numerical study, the parametric 3D geometry model can precisely reconstruct the aforementioned geometry within a valid error range. The hydrodynamic error analysis demonstrates that the geometric inaccuracy from the reconstructed model has less impact on the propeller performance. This indicates that the model described in this study is generalised and robust. Moreover, some uncommon propeller CAD models were generated in batches using the parametric 3D geometry model.

Keywords: marine propeller; geometric modeling; parametric 3D geometry model; surface reconstruction

INTRODUCTION

For nearly a decade, there has been a lot of focus on propeller design. Król presented a simplified lifting surface method, replacing the 3D task for the full blade with a series of 2D tasks for accomplishing blade section profiles [1]. Moreover, Król also analysed the uncertainty of full-scale propeller open water performance testing [2]. Nadery et al. used a numerical method to study the hydrodynamic performance of aft propellers with and without wake equalisation ducts

[3]. Greeley used numerical approaches for the design and study of propellers [4]. Recently, simulation-based design (SBD) has been widely applied in the naval architecture design field [5]-[11]. The geometry parameterisation is critical in SBD. The parametric 3D geometry model will facilitate the automated modelling and optimisation design of the propeller [12]. However, the number of 3D geometric parametric models currently available for propeller design and design optimisation is relatively limited. These parametric models are usually associated with the specific parameters

that the researcher is trying to optimise so they are not directly applicable as common models to automatically construct CAD models of propellers. For example, Bertetta et al. described the camber and thickness distributions of a propeller with B-spline parametric curves [13]. Furthermore, most parameters employed in the parametric model are coordinates of control points, which have less physical significance. To achieve automatic parametric modelling of the propeller, Ye fitted the given data points with the least square method and constructed the propeller blade surface based on the B-spline curve and surface [14]. Vickers carried out coordinate conversion of propeller data points through computer programming, and further built the three-dimensional model of a propeller [15]. Kim focused on the geometric modelling steps of marine propeller blades, blade roots and propeller hubs. Further, a comprehensive analysis of the leaf surface and the leaf back was carried out [16]. Lee established a propeller surface modelling system that can connect the propeller blade surface and blade back by building the side. The final surface constructed by this system can maintain G1 continuity of the surface at the joint part [17]. Pérez-Arribas generated the B-spline surface representation of the propeller blade while reducing the number of control points used. The effectiveness of the proposed method was verified by using it to reconstruct the model and compare it with a benchmark model [18]. Arapakopoulos et al. provided two propeller mathematical expression methods based on non-uniform rational B-splines (NURBS) and T-splines, respectively. These methods can quickly and automatically generate effective geometric representations of marine propellers [19]. However, the number of parameters in these parametric models is high and there are some barriers to using them directly for design optimisation.

In this study, the parametric modelling of a marine propeller is achieved by constructing 3D point cloud data through the inspiration of reverse engineering combined with parametric ideas. The goal of this work is to reduce the number of free parameters needed for parametric modelling while maintaining generality. Initially, a thorough explanation of the parametric calculation method for the propeller point cloud and the reverse engineering technique for the propeller surface reconstruction is provided. Several examples of error validation studies are additionally employed to explain the

parametric model. Finally, some uncommon propeller CAD models were generated in batches via the developed model.

MATERIALS AND METHODS

Reverse engineering is a viable method to create a 3D virtual CAD model of an existing physical part. The reverse engineering process involves measuring an object and then reconstructing it as a 3D model. The measured data is usually represented as a point cloud [20]. The reverse engineering procedure can be characterised by the flowchart in Fig. 1.

In classical reverse engineering, the physical object can be measured using 3D scanning technologies like structured light digitisers, or industrial computerised tomography (CT) scanning. However, the surface point cloud of a propeller can usually be calculated using mathematical methods. The flowchart of the parametric 3D geometry model of a marine propeller based on reverse engineering is updated to Fig. 2.

PROPELLER BLADE 3D POINT CLOUD

In Fig. 2, the initial step is the parametric point cloud calculation of the propeller. There are three processes in constructing the 3D point cloud of the propeller: the initial point cloud, the deformation point cloud and the fine point cloud. The general steps in constructing the 3D point cloud of the propeller blade are shown in Algorithm 1.

Algorithm 1: General steps in constructing the 3D point cloud of the propeller blade

1	begin
2	H : defining the feature matrix associated with the propeller blade profile.
3	D: propeller diameter $\rightarrow R_N$.
4	Create initial point cloud based on Eq. (4).
5	R : defining the deformation feature matrix.
6	Create deformation point cloud based on Eq. (12) and Eq. (13).
7	Resample based on Eq. (14) \rightarrow fine point cloud.
8	end

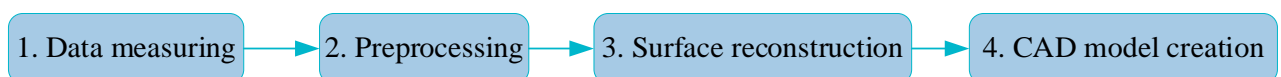


Fig. 1. Basic phases of reverse engineering

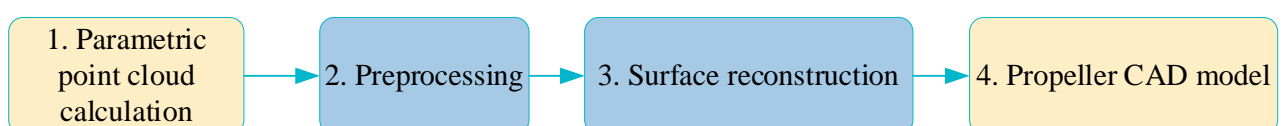


Fig. 2. Basic phases of parametric 3D geometry model of marine propeller based on reverse engineering

The computation process of the initial point cloud starts with defining the feature matrix associated with the propeller blade profile. The feature matrix is formulated as Eq. (1).

$$\mathbf{H} = \begin{bmatrix} H_{1,1} & H_{1,2} & \dots & H_{1,i} \\ H_{2,1} & H_{2,2} & \dots & H_{2,i} \\ \dots & \dots & \dots & \dots \\ H_{N,1} & H_{N,2} & \dots & H_{N,i} \end{bmatrix} \quad i = 1,2 \dots 8, N = 1,2 \dots \quad (1)$$

where N is the number of blade profiles composing the blade.

The initial point cloud is generated from \mathbf{H} according to Eq. (2) to (4).

(2)

$$\mathbf{X}_N = [0, \mathbf{H}_{N,1} * \cos(\mathbf{H}_{N,2}), 1 - \mathbf{H}_{N,3} * \cos(\mathbf{H}_{N,4}), 1, 1 - \mathbf{H}_{N,5} * \cos(\mathbf{H}_{N,6}), \mathbf{H}_{N,7} * \cos(\mathbf{H}_{N,8}), 0]$$

(3)

$$\mathbf{Y}_N = [0, \mathbf{H}_{N,1} * \sin(\mathbf{H}_{N,2}), \mathbf{H}_{N,3} * \sin(\mathbf{H}_{N,4}), 0, \mathbf{H}_{N,5} * \sin(\mathbf{H}_{N,6}), \mathbf{H}_{N,7} * \sin(\mathbf{H}_{N,8}), 0]$$

$$\mathbf{IP} = \begin{bmatrix} \mathbf{IPX} \\ \mathbf{IPY} \\ \mathbf{IPZ} \end{bmatrix} = \begin{bmatrix} \sum_{i=0}^3 N_{i,3}(u) \mathbf{X}_N(i) & \sum_{i=0}^3 N_{i,3}(u) \mathbf{X}_N(i+3) \\ \sum_{i=0}^3 N_{i,3}(u) \mathbf{Y}_N(i) & \sum_{i=0}^3 N_{i,3}(u) \mathbf{Y}_N(i+3) \\ R_N & R_N \end{bmatrix} \quad (4)$$

where u [0,0,0,0,1,1,1,1]. $N_{i,3}(u)$ is the De Boor Cox function [21][22]. R_n is the radius of the propeller, such as $0.2r/R, 0.3r/R \dots 0.9r/R, 1r/R$.

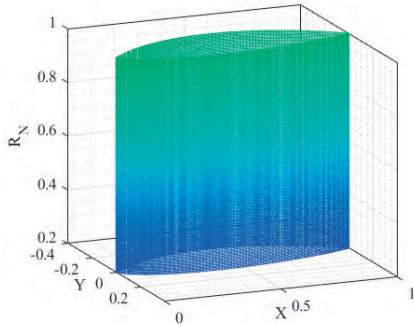


Fig. 3. Schematic diagram of initialised point cloud

The shape of the initialised point cloud is a ‘‘columnar’’ structure, similar to an airplane wing, as shown in Fig. 3. Therefore, a deformation feature matrix needs to be defined to deform the initialised point cloud. The deformation feature matrix is written as Eq. (5).

$$\mathbf{R} = \begin{bmatrix} R_{1,1} & R_{1,2} & \dots & R_{1,i} \\ R_{2,1} & R_{2,2} & \dots & R_{2,i} \\ \dots & \dots & \dots & \dots \\ R_{N,1} & R_{N,2} & \dots & R_{N,i} \end{bmatrix} \quad i = 1,2 \dots 6, N = 1,2 \dots 4 \quad (5)$$

where $R_{N,i}$ is the feature parameters of the propeller’s chord distribution, rake distribution, skew distribution, and pitch distribution. The detailed explanation is given in the appendix.

The deformation process of the initialised point cloud is based on Eq. (6) to (13).

(6)

$$\mathbf{X}_i = [R_{root}, R_{root} + R_{i,2} * \cos(R_{i,3}), R_{tip} - R_{i,4} * \cos(R_{i,5}), R_{tip}]$$

(7)

$$\mathbf{Y}_i = [R_{i,1}, R_{i,1} + R_{i,2} * \sin(R_{i,3}), R_{i,6} + R_{i,4} * \sin(R_{i,5}), R_{i,6}]$$

$$\begin{aligned} RCX(t)_i &= \mathbf{X}_i(1)(1-t)^3 + 3\mathbf{X}_i(2)t(1-t)^2 + \\ &+ 3\mathbf{X}_i(3)t^2(1-t) + \mathbf{X}_i(4)t^3, t \in [0,1] \end{aligned} \quad (8)$$

$$\begin{aligned} RCY(t)_i &= \mathbf{Y}_i(1)(1-t)^3 + 3\mathbf{Y}_i(2)t(1-t)^2 + \\ &+ 3\mathbf{Y}_i(3)t^2(1-t) + \mathbf{Y}_i(4)t^3, t \in [0,1] \end{aligned} \quad (9)$$

where R_{root} is the radius ratio at the propeller blade root, the recommended value of which is $0.2r/R$. The same R_{tip} is the radius ratio at the blade tip. $i=1, \dots, 4$, meaning the chord distribution, skew distribution, rake distribution, and pitch distribution, respectively.

$$UCX(u)'_N = \mathbf{IPX} * RCX(t_N)_1 \quad (10)$$

$$LCX(u)'_N = \mathbf{IPY} * RCX(t_N)_1 \quad (11)$$

where N is the n -th section in the radial direction of the propeller, and is the chord distribution function.

$$\begin{aligned} Xu_N &= -[RCX(t_N)_2 + RCX(t_N)_3 * \tan(RCX(t_N)_4)] + (0.5 * RCX(t_N)_1 - UCX(u)'_N) \\ &* \sin(RCX(t_N)_4) + UCY(u)'_N * \cos(RCX(t_N)_4) \\ Yu_N &= \sin[RCX(t_N)_3 - (0.5 * RCX(t_N)_1 - UCX(u)'_N) * \cos(RCX(t_N)_4) - UCY(u)'_N \\ &* \sin(RCX(t_N)_4)] \\ Zu_N &= \cos[RCX(t_N)_3 - (0.5 * RCX(t_N)_1 - UCX(u)'_N) * \cos(RCX(t_N)_4) - UCY(u)'_N \\ &* \sin(RCX(t_N)_4)] \\ Xl_N &= -[RCX(t_N)_2 + RCX(t_N)_3 * \tan(RCX(t_N)_4)] + (0.5 * RCX(t_N)_1 - LCX(u)'_N) \\ &* \sin(RCX(t_N)_4) + LCY(u)'_N * \cos(RCX(t_N)_4) \end{aligned} \quad (12)$$

$$\begin{aligned} Yl_N &= \sin[RCX(t_N)_3 - (0.5 * RCX(t_N)_1 - LCX(u)'_N) * \cos(RCX(t_N)_4) - LCY(u)'_N \\ &* \sin(RCX(t_N)_4)] \\ Zl_N &= \cos[RCX(t_N)_3 - (0.5 * RCX(t_N)_1 - LCX(u)'_N) * \cos(RCX(t_N)_4) - LCY(u)'_N \\ &* \sin(RCX(t_N)_4)] \end{aligned} \quad (13)$$

The $Xu_N, Yu_N, Zu_N, Xl_N, Yl_N, Zl_N$ form the form the deformation point cloud. It should be noted that when

defining H , N in Eq. (1) usually takes the value of 10, that is, ten blade sections are used to express the propeller blade. This results in sparse initialisation point clouds and distorted point clouds. Therefore, the sparse deformed point cloud is refined by resampling. The resampling method is written as Eq. (14).

$$\begin{bmatrix} X_N^{re} \\ Y_N^{re} \\ Z_N^{re} \end{bmatrix} = \begin{bmatrix} M-j \\ M \\ j \\ M \end{bmatrix} \begin{bmatrix} X_N^{i+1} - X_N^i \\ Y_N^{i+1} - Y_N^i \\ Z_N^{i+1} - Z_N^i \end{bmatrix} \quad (14)$$

where $j = 1, 2, \dots, M$. M is the number of the resample.

Fig. 4 summarises the aforementioned procedure using an example of a propeller with a diameter of 2.5 m. Interactively defining H , R , and D leads to the parametric production of 3D point clouds for propellers.

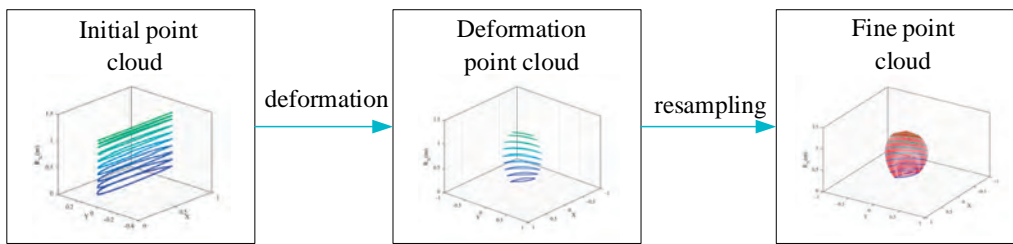


Fig. 4. Phases of creating parametric point cloud of propeller

SURFACE RECONSTRUCTION TO FORM POINT CLOUD

There is essentially no noise data since the point cloud data in this study was produced using mathematical techniques. As a result, the traditional surface reconstruction methodology based on the moving least squares (MLS) method [23][24] can be utilised to conclude the propeller's surface reconstruction. The basic idea of using the MLS for surface reconstruction is to grid the reconstruction area first, then calculate the node values on the grid points, and finally connect the grid nodes to form a surface. Algorithm 2 shows the process of surface reconstruction. The specific properties of this method are described in the literature [23][24].

Algorithm 2: Surface reconstruction based on MLS

1	begin
2	Grid the reconstruction area.
3	for =1: n (Number of grid points) do
4	Determine the area of influence of grid points.
5	Determine the nodes of the area of influence.
6	Compute shape functions.
7	Compute the node value at the grid point.
8	end
9	Connect mesh points to form surface.
10	end

ANALYSIS AND VERIFICATION

SHAPE ERROR ANALYSIS

This work aims to reconstruct the propeller geometry by using a parametric 3D geometry model of a marine propeller based on reverse engineering. Therefore, the shape error analysis of the propeller reconstruction will be performed. The shape error is represented by the distance between the offset and the surface of the propeller. In this analysis, two typical propellers, AU series and B series, are chosen as the research objects. Table 1 lists the main parameters of the propellers.

Tab. 1. General parameters for the construction of a generic marine propeller

Item	AU series	B series
Diameter (m)	2.5	2.5
Number of sections	4	4
Area ratio	0.55	0.55
Pitch ratio	1.00	1.00

Fig. 5 shows the propeller constructed using the method proposed in this article and the corresponding offset. Similarly, the shape errors of the two propellers are also depicted in Fig. 5.

As shown in Fig. 5, at the part of the face side, the maximum error positions for the AU series and B series at each radius are close to the leading edge of the blade section. At the part of the back side, the distance error of the AU series and B series is relatively evenly distributed on each radius. Comparatively, Fig. 5 further demonstrates that the error near the blade root is larger than the error at the tip. The error of the blade back side is greater than the error of the blade face side when the method proposed in this paper is used to construct the aforementioned propeller. The highest deviation for all the propellers that were previously reconstructed is commonly less than 0.2 m (8% D). As a consequence, the method described in this research can be applied to the geometric representation and reconstruction of propellers with high precision and flexibility. All of the aforementioned shape errors, taken collectively, fall within a fair range of engineering standards.

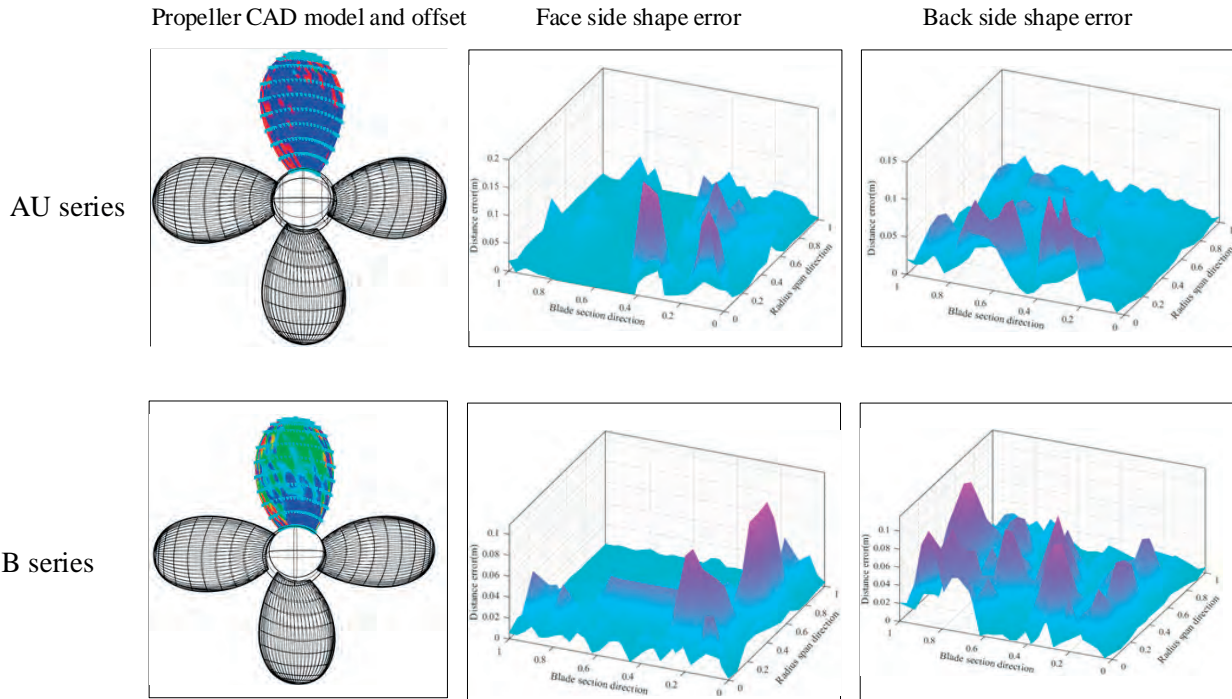


Fig. 5. The shape error of AU series and B series

HYDRODYNAMIC PERFORMANCE ERROR ANALYSIS

The purpose of the marine propeller CAD model is to design or optimise the propeller. Therefore, the primary focus of this analysis is to investigate whether the shape error produced during the reconstruction of the propeller model will have a seriously negative effect on the propeller's hydrodynamic performance. The specific operation for hydrodynamic performance error analysis is to operate computational fluid dynamics (CFD) simulations on both the reconstructed propeller model at a scale of 10 and the benchmark propeller model, also at a scale of 10, and then to investigate whether the distance error generated by the reconstruction will lead to a large performance error by comparing the error between the open water performance

obtained by CFD calculation. The grid reliability analysis, boundary condition setting, and solver settings involved in the numerical calculation refer to previous publications [25][26][27]. The open water performance of the propeller obtained by the CFD solver of the reconstructed propeller and the benchmark propeller is shown in Fig. 6. Fig. 6 (a) is the open water performance for the AU series, and Fig. 6 (b) is the open water performance for the B series. As observed in Fig. 6, the reconstructed AU series and benchmark propeller exhibit considerable hydrodynamic performance differences, whereas the reconstructed B series and prototype propeller exhibit similar hydrodynamic performance. This matches with Fig. 5. In terms of the distance error between the benchmark propeller and the reconstructed propeller, the error of the AU series is greater than that of the B series.

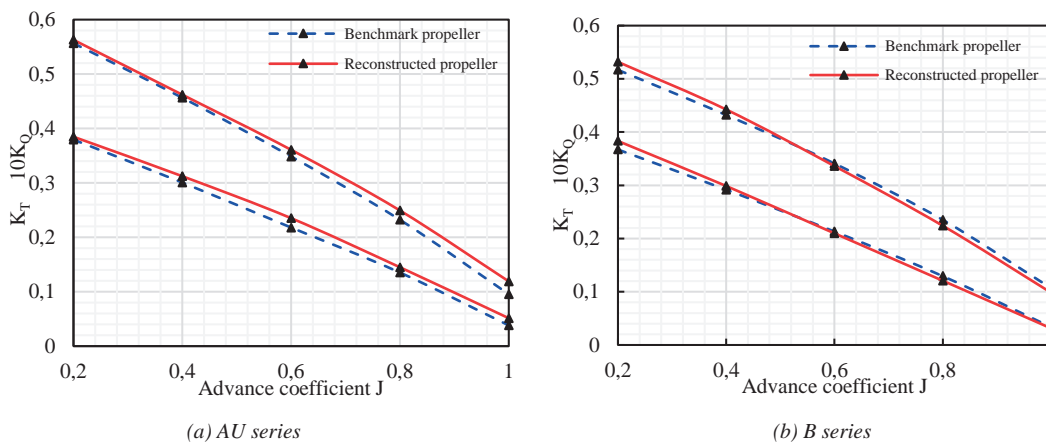


Fig. 6. Open water performance curve obtained by CFD

In addition, when the propeller works, the pressure at the blade back decreases to form a suction surface. Cavitation will take place if the pressure at a particular location falls below the critical level. The pressure distribution on the propeller surface will have a great impact on the cavitation performance of the propeller. Therefore, in order to investigate whether

the errors generated during the reconstruction will lead to drastic changes in the pressure distribution of the propeller, the pressure distribution of the benchmark propeller and the reconstructed propeller at the corresponding advance coefficient (J) is shown in Fig. 7 to Fig. 9.

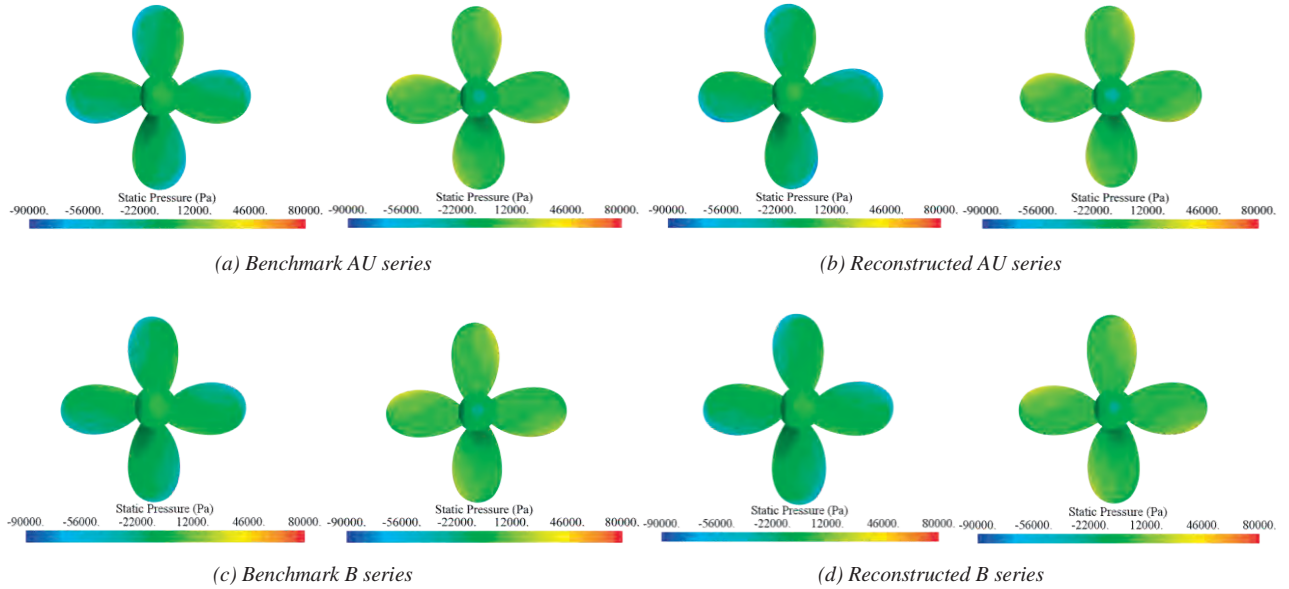


Fig. 7. Pressure distribution of benchmark blade and reconstructed blade ($J=0.4$)

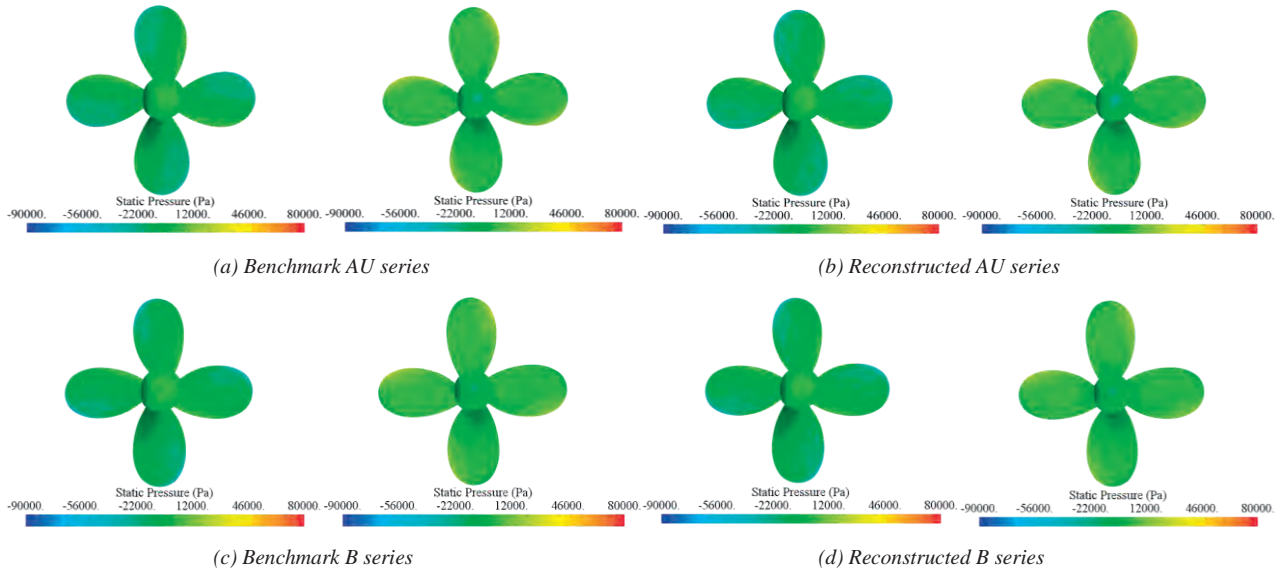


Fig. 8. Pressure distribution of benchmark blade and reconstructed blade ($J=0.6$)

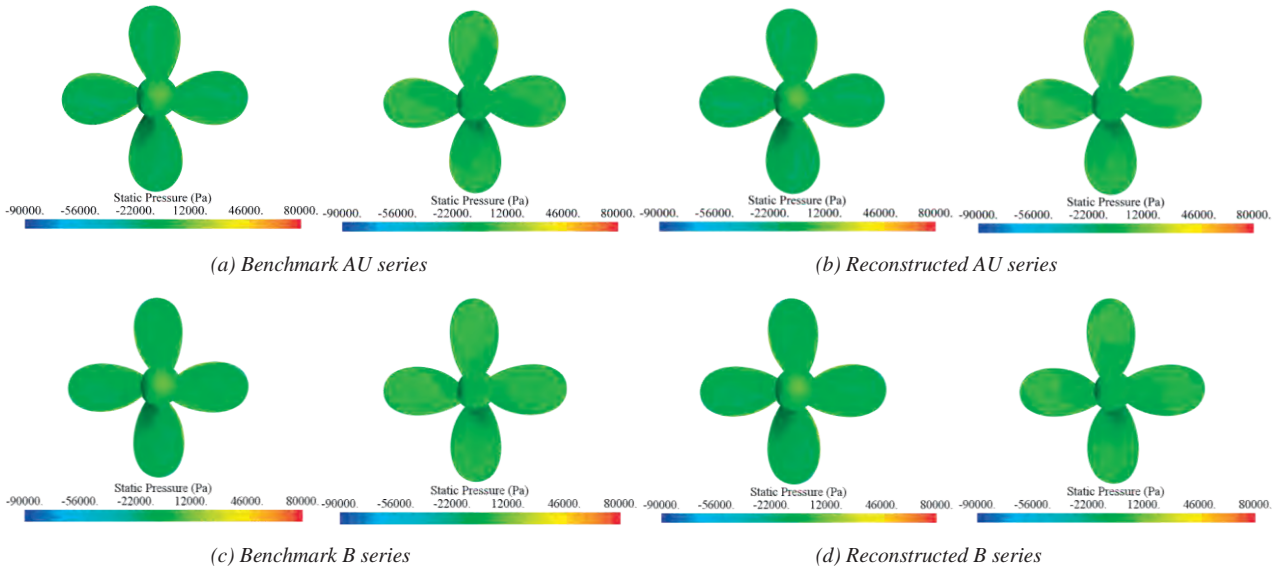


Fig. 9. Pressure distribution of benchmark blade and reconstructed blade ($J=0.8$)

Fig. 7 to Fig. 9 show that the surface pressure distribution of the reconstructed propeller is not significantly different from that of the benchmark propeller. In order to further investigate the variation of the pressure distribution, the pressure coefficients at different radii as the advance coefficient increases are given in Fig. 10 to Fig. 12, which show that, for various advance speed coefficients, the pressure distribution change of $0.6 r/R$ is rather minimal. Moreover, when $J=0.4$, the change in the AU series' pressure distribution is more visible than the change in the B series, when $J=0.6$,

the change in the AU series is also merely moderately obvious and when $J=0.8$, the B series is relatively larger. The results indicate that the geometric error produced when utilising the method proposed in this paper to reconstruct the propeller geometric model does not significantly affect the reconstructed propeller's performance (including open water performance and pressure distribution). As a consequence, it can be demonstrated that the method presented in this research can be utilised to deform and reconstruct propeller geometry in an efficient manner.

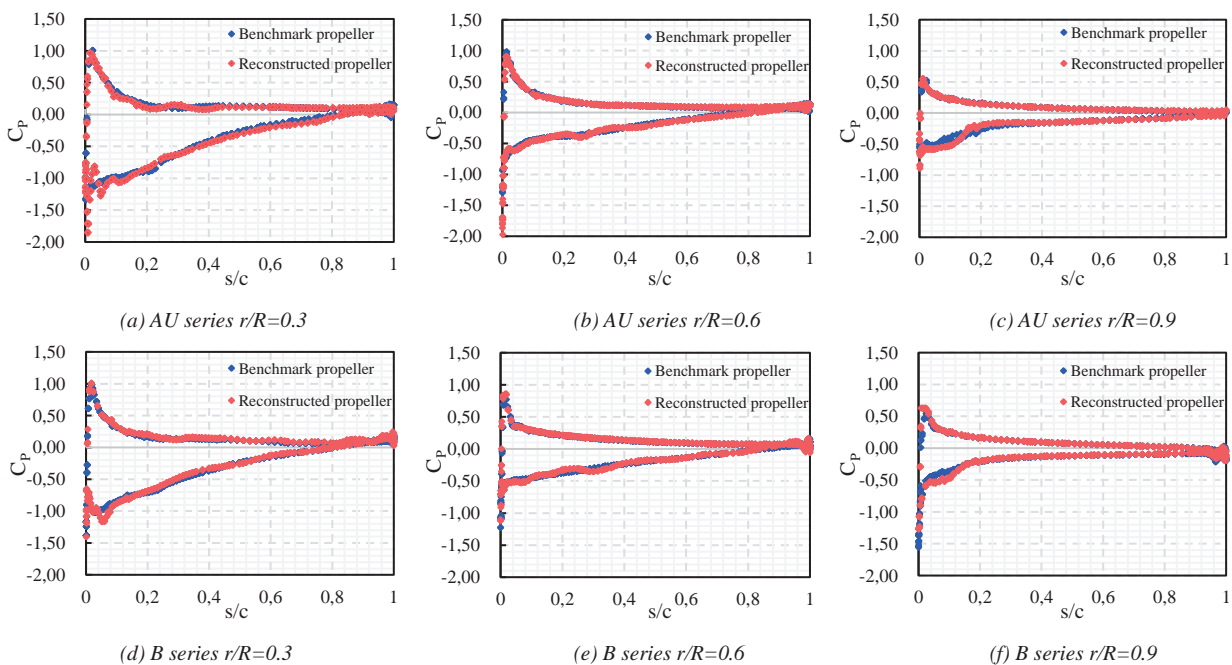


Fig. 10. Pressure coefficient at $J=0.4$

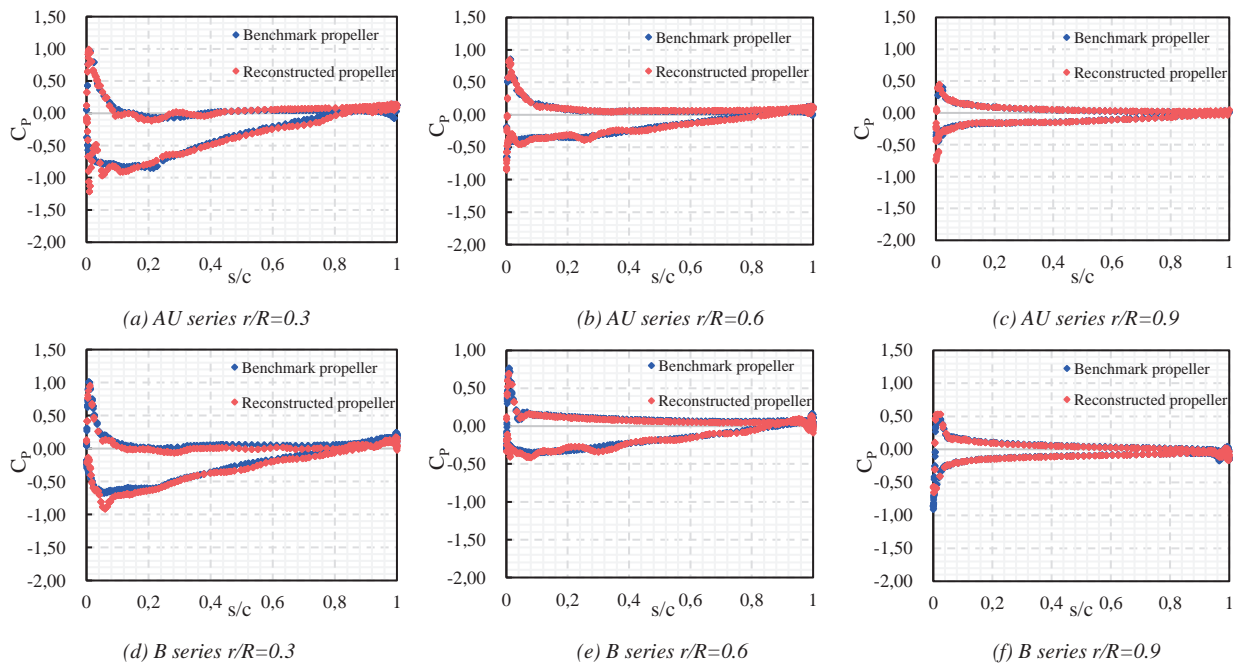


Fig. 11. Pressure coefficient at $J=0.6$

APPLICATION OF PARAMETRIC

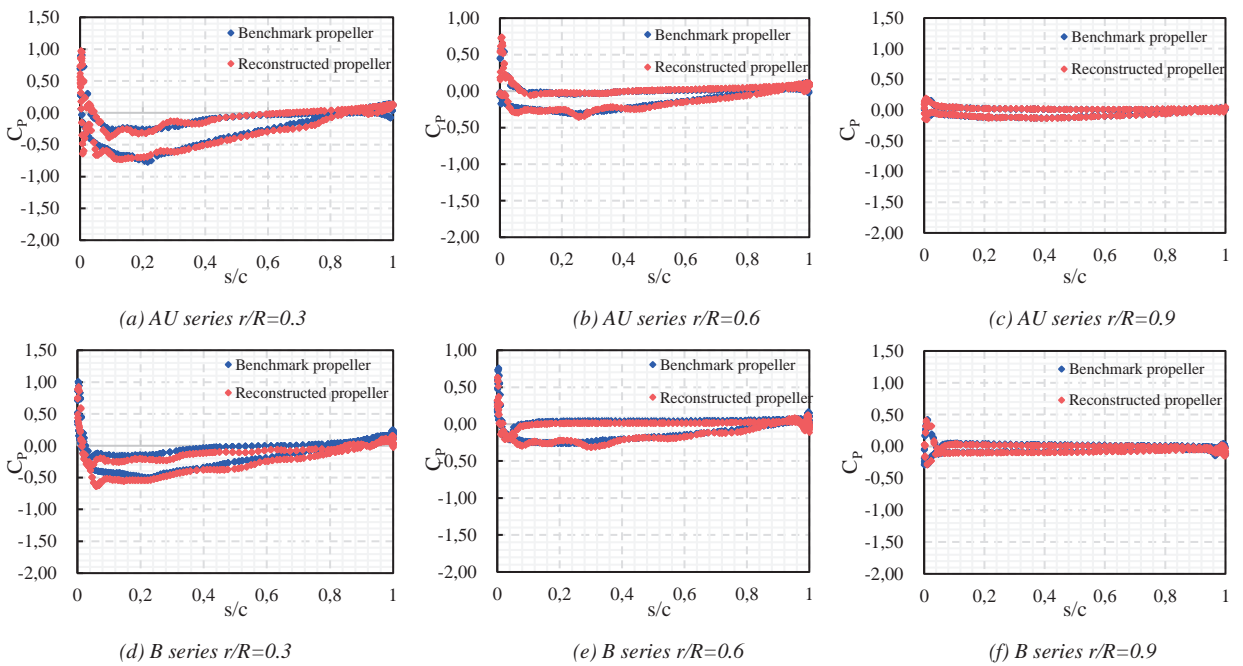


Fig. 12. Pressure coefficient at $J=0.8$

CONSTRUCTION OF PROPELLER

In theory, an infinite number of propeller CAD models can be generated by different combinations of feature parameters. In practical engineering applications, the propeller CAD model often needs to be generated under specific constraints. In this part using NACA 66 as the blade profile (constraint), the initial point cloud is generated; thus, \mathbf{H} remains unaltered and constant, and several propeller CAD models are produced by specifying various \mathbf{R} . \mathbf{R} contains 24 parameters, among which and represent the information at the propeller blade root and blade tip, which are also unchanged as constraints. The remaining 16 parameters are used as design variables, and the upper and lower bounds are listed in Table 2. The diameter (D) of the generated propellers is 0.25 m. The values of the constraint parameters (and) are listed in Table 3.

Tab. 2. Boundaries of design variables used for sample generation

NO.	Name	Lower Bound	Upper Bound
1	$R_{1,2}$	0.001	0.15
2	$R_{1,3}$	30°	90°
3	$R_{1,4}$	0.05	0.2
4	$R_{1,5}$	80°	90°
5	$R_{2,2}$	0.001	0.09
6	$R_{2,3}$	0°	5°
7	$R_{2,4}$	0.001	0.02
8	$R_{2,5}$	0°	5°
9	$R_{3,2}$	0.001	0.09
10	$R_{3,3}$	-10°	10°
11	$R_{3,4}$	0.001	0.02

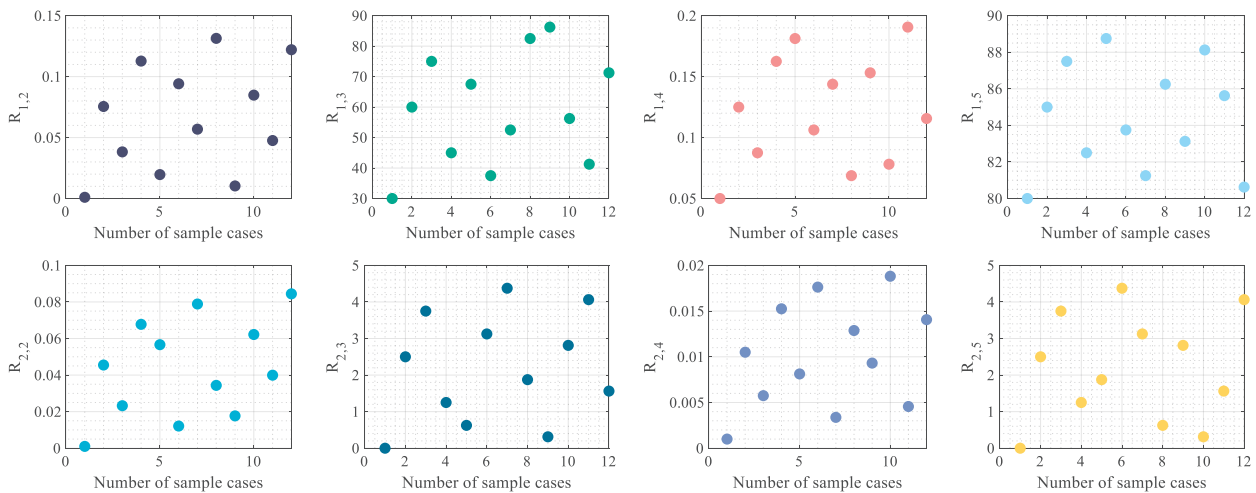
NO.	Name	Lower Bound	Upper Bound
12	$R_{3,5}$	0°	10°
13	$R_{4,2}$	0.001	0.09
14	$R_{4,3}$	0°	10°
15	$R_{4,4}$	0.001	0.02
16	$R_{4,5}$	0°	10°

Tab. 3. Values of constraint parameters

NO.	Name	Value
1	$R_{1,1}$	0.058
2	$R_{1,6}$	0
3	$R_{2,1}$	0°
4	$R_{2,6}$	0°
5	$R_{3,1}$	-4.72°
6	$R_{3,6}$	24.18°
7	$R_{4,1}$	0.209
8	$R_{4,6}$	0.209

The design variables were sampled using the Sobol algorithm [28]. With the aim of uniformly sampling the design space, this technique propagates the design solution throughout the variable domain space in a standard manner by using a Sobol sequence that imitates the behaviour of a series of random numbers. The technique can cover the full design area and is primarily utilised for experimental ideas.

The Sobol algorithm was used to randomly select 12 samples within that range as cases. Fig. 13 shows the distribution of the parameters in their respective value ranges.



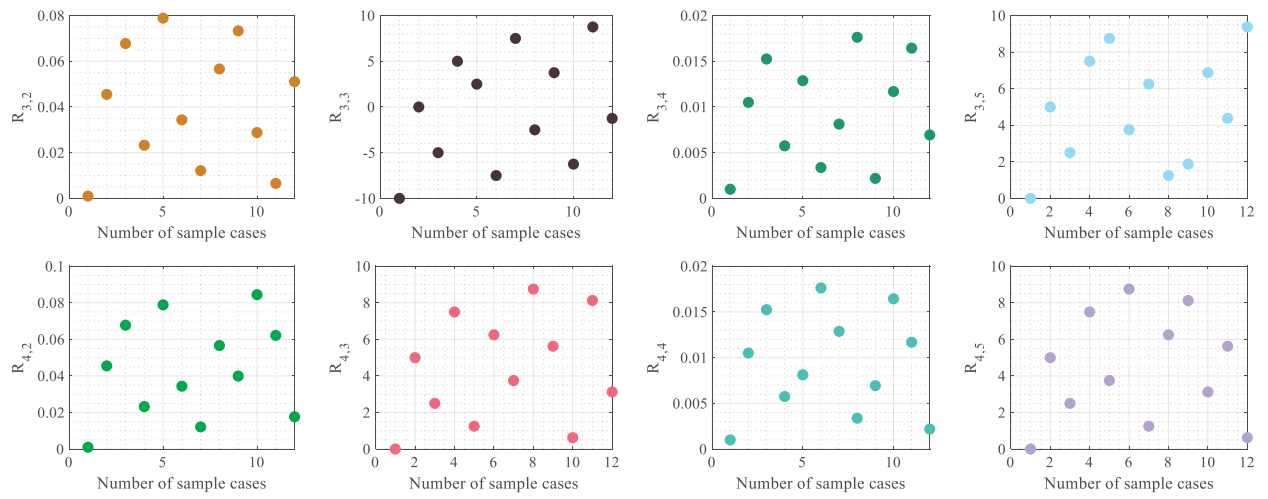


Fig. 13. Distribution of design variables in space

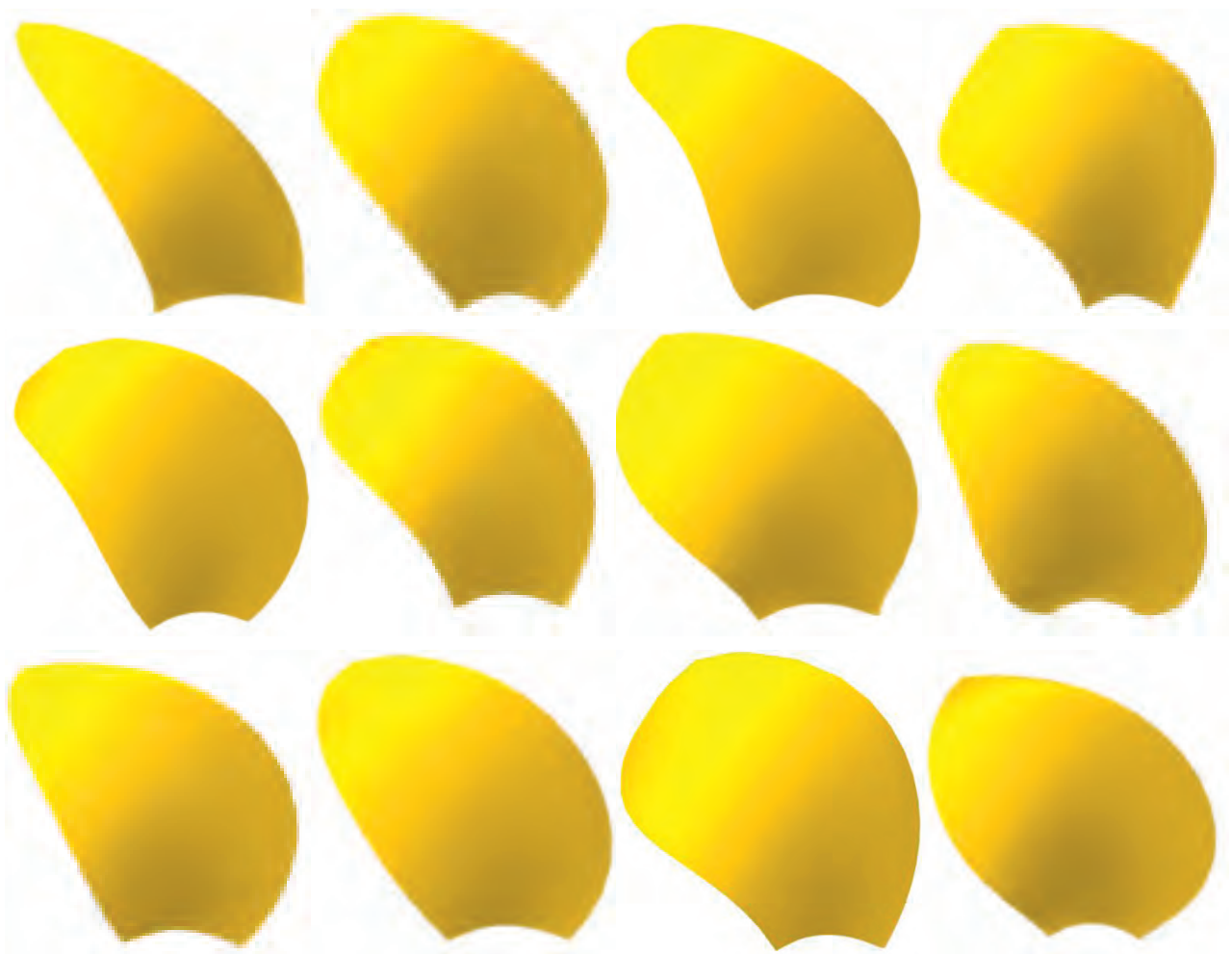


Fig. 14. Propeller blade model for each case

According to the combination of parameters corresponding to each case, the CAD model is driven to automatically generate the corresponding propeller. Fig. 14 depicts the propeller geometry model corresponding to each case. It can be seen that the model in this article can construct a series of uncommon propeller geometries to help designers explore novel design space.

CONCLUSION AND FUTURE WORKS

In this article, a parametric 3D geometry model of a marine propeller is constructed. The basic idea of the model is inspired by reverse engineering. The point cloud of the propeller generated is parameterised by a mathematical calculation method. The surface reconstruction algorithm based on MLS is used to generate the propeller surface. Different propeller CAD models can be built smoothly by modifying the corresponding parameters interactively. By using this technique, the parameter-driven creation of propeller surfaces is realised. This may quickly supply designers with a large number of sample propellers, saving the time required for manual modelling and modification, considerably increasing design efficiency, and offering certain engineering benefits. Simultaneously, the propellers created by this technique have good smoothness and satisfy the fundamental design criteria, so they can be utilised as the foundational model for subsequent performance investigation. In future research, we will work on the feature extraction of the parameters in this model by means of sensitivity analysis and feature selection methods. In addition, we hope to combine feature selection work to realise a propeller automation optimisation framework that comprehensively considers propeller efficiency, propeller cavitation and propeller vibration noise.

FUNDING SOURCES

This work was supported by Research and Development of Key Technologies for the Design of River and Coastal Connection on the Pinglu Canal (NNZC2023-G3-990158-GSXX) and the Innovation Research Foundation of Ship General Performance (30222221).

DECLARATION OF COMPETING INTEREST

The authors declare that they have no known competing financial interests or personal relationships that could have appeared to influence the work reported in this paper.

REFERENCES

1. P. Król, "Blade section profile array lifting surface design method for marine screw propeller blade," *Polish Maritime Research*, vol. 26, no. 4, 3919, pp.134-141, 2019. doi: /10.2478/pomr-2019-0075.

2. P. Król, "Analysis of model-scale open-water test uncertainty," *Polish Maritime Research*, vol. 29, no. 4, 3922, pp. 4-11, 2022. doi: /10.2478/pomr-2022-0039.
3. A. Nadery and H. Ghassemi, "Numerical investigation of the hydrodynamic performance of the propeller behind the ship with and without Wed," *Polish Maritime Research*, vol. 27, no. 4, 3920, pp. 50-59, 2020. doi: /10.2478/pomr-2020-0065.
4. D. S. Greeley, "Numerical method for propeller design and analysis in steady flow," *SNAME Transactions*, vol. 90, pp. 415-453, 1982.
5. M. Diez, A. Serani, E. F. Campana, et al., "Design space dimensionality reduction for single-and multi-disciplinary shape optimization," *Proceedings of AIAA/ISSMO Multidisciplinary Analysis and Optimization Conference (MA&O). AVIATION 2016*, Washington DC, USA. 13-17 June, 2016. doi: 10.2514/6.2016-4295.
6. I. Marinić-Kragić, D. Vučina, and M. Ćurković, "Efficient shape parameterization method for multidisciplinary global optimization and application to integrated ship hull shape optimization workflow," *Computer-Aided Design*, vol. 80, 2016, ISSN 0010-4485. doi: 10.1016/j.cad.2016.08.001.
7. A. Miao, M. Zhao, and D. Wan, "CFD-based multi-objective optimisation of S60 Catamaran considering demihull shape and separation," *Applied Ocean Research*, vol. 97, 2020. doi:10.1016/j.apor.2020.102071.
8. A. Serani, F. Stern, E. F. Campana, et al., "Hull-form stochastic optimization via computational-cost reduction methods," *Engineering with Computers*, vol. 38 (Suppl. 3), pp. 2245-2269, 2022. doi:10.1007/s00366-021-01375-x.
9. S. Gaggero, "Numerical design of a RIM-driven thruster using a RANS-based optimization approach," *Applied Ocean Research*, vol. 94, 101941, 2020. doi:10.1016/j.apor.2019.101941.
10. S. Gaggero, J. Gonzalez-Adalid, and M. P. Sobrino, "Design and analysis of a new generation of CLT propellers," *Applied Ocean Research*, vol. 59, pp. 424-450, 2016. doi:10.1016/j.apor.2016.06.014.
11. S. Gaggero, G. Tani, D. Villa, M. Viviani, P. Ausonio, P. Travi, G. Bizzarri, and F. Serra, "Efficient and multi-objective cavitating propeller optimization: An application to a high-speed craft," *Applied Ocean Research*, vol. 64, pp. 31-57, 2017. doi:10.1016/j.apor.2017.01.018.
12. S. Gaggero, G. Vernengo, and D. Villa, "A marine propeller design method based on two-fidelity data levels," *Applied Ocean Research*, vol. 123, 103156, 2022. doi:10.1016/j.apor.2022.103156.

13. D. Bertetta, S. Brizzolara, S. Gaggero, M. Viviani, and L. Savio, "CPP propeller cavitation and noise optimization at different pitches with panel code and validation by cavitation tunnel measurements," *Ocean Engineering*, vol. 53, pp. 177-195, 2012. doi:10.1016/j.oceaneng.2012.06.026.
14. X. Ye, T. R. Jackson, and N. M. Patrikalakis, "Geometric design of functional surfaces," *Computer-Aided Design*, vol. 28, no. 9, pp. 741-52, 1996. doi:10.1016/0010-4485(95)00080-1.
15. G. W. Vickers, "Computer-aided manufacture of marine propellers," *Computer-Aided Design*, vol. 9, no. 4, pp. 267-74, 1977. doi:10.1016/0010-4485(77)90008-2.
16. Y. C. Kim, Y. M. Lee, M. J. Son, T. W. Kim, and J. C. Suh, "Generating cutter paths for marine propellers without interference and gouging," *Journal of Marine Science and Technology*, vol. 14, no. 3, pp. 275-84, 2009. doi:10.1007/s00773-008-0033-2.
17. C. S. Lee and J. H. Lee, "Geometric modeling and tool path generation of model propellers with a single setup change," *The International Journal of Advanced Manufacturing Technology*, vol. 50, no. 1, pp. 253-63, 2010. doi:10.1007/s00170-009-2495-8.
18. F. Pérez-Arribas and R. Pérez-Fernández, "B-spline design model for propeller blades," *Advances in Engineering Software*, vol. 118, pp. 35-44, 2018. doi:10.1016/j.advengsoft.2018.01.005.
19. A. Arapakopoulos, R. Polichshuk, Z. Segizbayev, S. Ospanov, A. I. Ginnis, and K. V.Kostas, "Parametric models for marine propellers," *Ocean Engineering*, vol. 192, 106595, 2019. doi:10.1016/j.oceaneng.2019.106595.
20. T. Várady, R. R. Martin, and J. Cox, "Reverse engineering of geometric models—an introduction," *Computer-Aided Design*, vol. 29, no. 4, pp. 255–268, 1997. doi:10.1016/s0010-4485(96)00054-1.
21. M. G. Cox, The numerical evaluation of B-splines. Technical report, National Physics Laboratory DNAC 4, 1971. doi:10.1093/imamat/10.2.134.
22. C. De Boor, "On calculation with B-splines," *Journal of Approximation Theory*, vol. 6, pp. 50–62, 1972. doi:https://doi.org/10.1016/0021-9045(72)90080-9.
23. P. Lancaster and K. Salkauskas, "Surfaces generated by moving least squares methods," *Mathematics of Computation*, vol. 37, no. 155, pp. 141-158, 1981. doi:10.2307/2007507.
24. Q. H. Zeng and D. T. Lu, "Curve and surface fitting based on moving least-squares methods," *Journal of Engineering Graphics*, vol. 25, no. 1, pp. 84-89, 2004. doi:1003-0158(2004)01-0084-06.
25. A. Yazaki, E. Kuramochi, and T. Kumasaki, "Open water test series with modified AU-type four-bladed propeller models," *Journal of Zosen Kiokai*, vol. 108, pp. 99-104, 1960.
26. S. Leone, C. Testa, L. Greco, and F. Salvatore, "Computational analysis of self-pitching propellers performance in open water," *Ocean Engineering*, vol. 64, pp. 122-134, 2013. doi:https://doi.org/10.1016/j.oceaneng.2013.02.012.
27. W. Zhu and H. Gao, "Hydrodynamic characteristics of bioinspired marine propeller with various blade sections," *Ships and Offshore Structures*, 2020. doi:10.1080/17445302.2020.1713039.
28. S. Joe and F. Y. Kuo, "Remark on Algorithm 659: Implementing Sobol's Quasirandom Sequence Generator," *ACM Transactions on Mathematical Software*, vol. 29, no. 1, pp. 49–57, 2003. doi:10.1145/42288.214372.

APPENDIX

PHYSICAL MEANING OF PARAMETERS IN H AND R

H is related to the blade profile shape of the propeller. These parameters are provided in Table 4.

Tab. 4. Parameters used in blade profile shape

Nr.	Name	Symbol
0	Chord	L
1	Upper-side leading edge shift length	$H_{N,1}$
2	Upper-side leading edge angle of advance	$H_{N,2}$
3	Upper-side trailing edge shift length	$H_{N,3}$
4	Upper-side trailing edge angle of departure	$H_{N,4}$
5	Lower-side leading edge shift length	$H_{N,5}$
6	Lower-side leading edge angle of advance	$H_{N,6}$
7	Lower-side trailing edge shift length	$H_{N,7}$
8	Lower-side trailing edge angle of departure	$H_{N,8}$
Note:	<p>The angle at the leading edge point, specified as the positive direction of the x-axis, is 0 degrees, the clockwise direction is negative, and the counterclockwise direction is positive.</p> <p>The angle at the trailing edge point, specified as the negative direction of the x-axis, is 0 degrees, the clockwise direction is positive, and the counterclockwise direction is negative.</p>	

The coordinate system needs to be specified. Assuming that the origin of the coordinate system is at the leading edge point of the hydrofoil, the longitudinal axis coincides with the line connecting the leading edge point and the trailing edge point, and the positive direction is toward the trailing edge. Fig. 15 shows the corresponding meanings of each parameter. The ordinates of the hydrofoil's upper side will always be non-negative numbers, while the lower side values can be either negative or mixed, depending on the hydrofoil's camber.

(15)

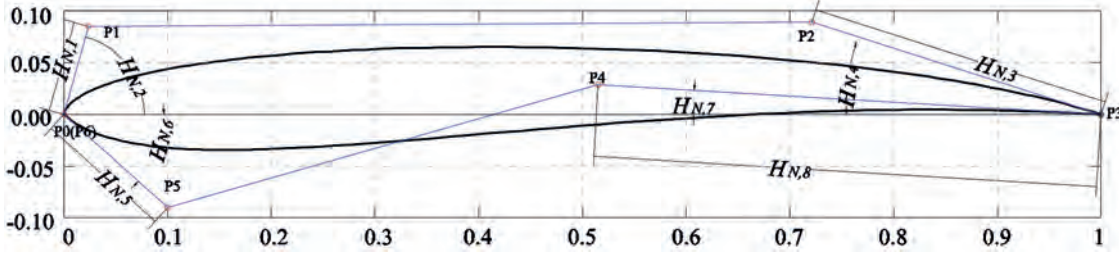


Fig. 15. Schematic diagram of feature parameters

R is related to the radial distribution of the propellers. These radial distributions include the chord distribution, rake distribution, skew distribution and pitch distribution. The definitions of the parameters in R are listed in Table 5. Fig. 16 shows a graphical explanation of the corresponding parameters.

Tab. 4. Parameters used in radial distribution

Nr.	Name	Symbol
1	The value of the root	$R_{N,1}$
2	Corresponding radial parameters, leading edge shift length	$R_{N,2}$
3	Corresponding radial parameters, angle of advance	R
4	Corresponding radial parameters, trailing edge shift length	$R_{N,4}$
5	Corresponding radial parameters, angle of departure	$R_{N,5}$
6	The value of the tip	$R_{N,6}$

Note:
 The angle at the leading edge point, specified as the positive direction of the x-axis, is 0 degrees, the clockwise direction is negative, and the counterclockwise direction is positive.
 The angle at the trailing-edge point, specified as the negative direction of the x-axis, is 0 degrees, the clockwise direction is positive, and the counterclockwise direction is negative.

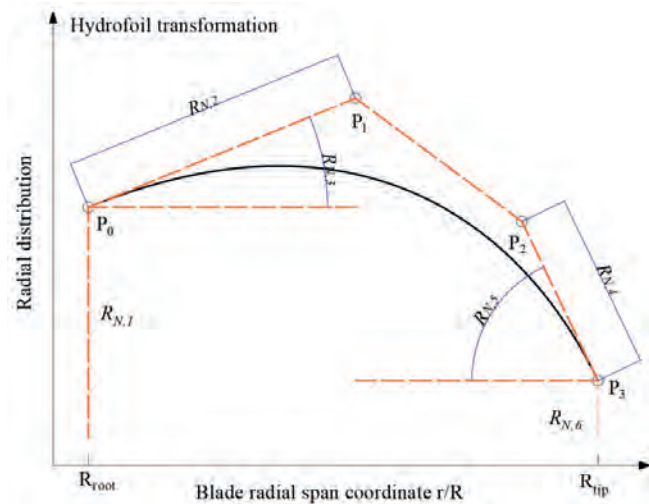


Fig. 16. Schematic diagram of feature parameters

The relationship between R and the propeller parameters (propeller area ratio, pitch, skew, rake) is shown in Eq. (15) to Eq. (20).

(16)

$$P_N: x = [R_{root}, R_{root} + R_{N,2} * \cos(R_{N,3}), R_{tip} - R_{N,4} * \cos(R_{N,5}), R_{tip}]$$

(17)

$$P_N: y = [R_{N,1}, R_{N,1} + R_{N,2} * \sin(R_{N,3}), R_{N,6} + R_{N,4} * \sin(R_{N,5}), R_{N,6}]$$

$$\frac{A_e}{A_0} = \frac{4Z \int_{r_n}^R \sum_{i=0}^3 C_3^i P_1^i (1-t(x))^{3-i} (t(x))^i dr}{\pi D^2} \quad (18)$$

$$Rake = P_2^3: y$$

$$Skew = P_3^3: y$$

$$\bar{P} = \frac{\int_{r_n}^R \sum_{i=0}^3 C_3^i P_4^i (1-t(x))^{3-i} (t(x))^i dr}{\int_{r_n}^R r dr} \quad (19)$$

$$\text{An example of } R = \begin{bmatrix} 0.66 & 0.65 & 20^\circ & 0.25 & 75^\circ & 0 \\ 0 & 0.5 & 0^\circ & 0.5 & 0^\circ & 0 \\ 0 & 0.5 & 0^\circ & 0.5 & 0^\circ & 0 \\ 0.6 & 0.5 & 0^\circ & 0.5 & 0^\circ & 0.6 \end{bmatrix} \quad (20)$$

is depicted in Fig. 17.

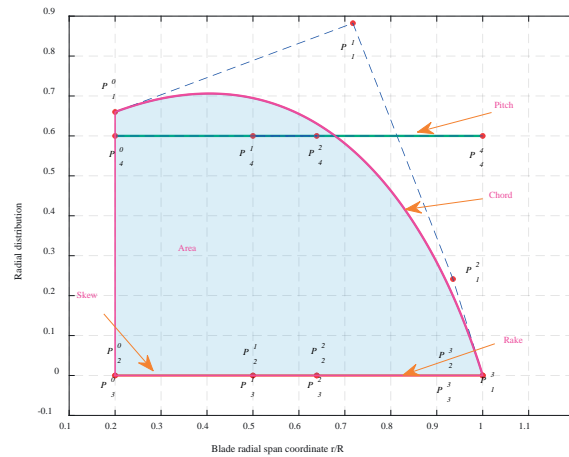


Fig. 17.. The radial parameter generated from the R

The rake and skew of this propeller are both 0, and the pitch of the fixed pitch propeller is constant along the span direction of the propeller.